

Applicability of APT Aided-Inertial System to Crustal Movement Monitoring

J. Arnold Soltz

The Charles Stark Draper Laboratory, Inc.
Cambridge, Massachusetts 02139

Abstract. The APT system, its stage of development, hardware, and operations are described. The algorithms required to perform the real-time functions of navigation and profiling are presented. The results of computer simulations demonstrate the feasibility of APT for its primary mission: topographic mapping with an accuracy of 15 cm in the vertical. Also discussed is the suitability of modifying APT for the purpose of making vertical crustal movement measurements accurate to 2 cm in the vertical, and at least marginal feasibility is indicated.

Introduction

The Charles Stark Draper Laboratory, Inc., under sponsorship of the U.S. Department of the Interior, Geological Survey*, is developing an airborne-instrument system capable of providing precisely located, geophysical data. This equipment, called APTS (Aerial Profiling of Terrain System), is designed to be carried by a relatively small maneuverable aircraft. It incorporates a surveying instrument package, unaffected by aircraft motion, capable of continuously providing a high-accuracy, three-coordinate position datum. A self-contained terrain-measuring device for recording the vertical position of the terrain below the aircraft is also provided for applications such as stream-valley profiling. A vidicon camera is to be boresighted with the terrain-measuring device to aid in the data processing. Performance goals call for locating an unsurveyed ground control point with respect to three or more established ground control points to an accuracy of ± 15 cm in the vertical coordinate and ± 60 cm in the horizontal coordinate.

The work completed to date consists of engineering analysis, system configuration design, mathematical analysis, and computer simulation, selection and specification of all major hardware components, mechanical design, thermal design and test, electronic design, subsystem interface design and specification, selection and recommendation of flight computer, analysis of flight strategy, specification and design of key flight algorithms, and, in addition, a flight test of a breadboard laser profiler. Within the time and funding resources available, the program has been organized so that a balanced effort has been maintained in the various aspects of system and subsystem design to facilitate an orderly transition into the fabrication, laboratory test, and flight trial of a test bed system.

The APT system is designed to function in a small aircraft at altitudes of 1,000 meters or less. The system is to be used for applications such as:

- (1) Producing topographic maps.
- (2) Testing the reliability of older published maps.
- (3) Fitting specified flood magnitudes into local stream-valley geometry.

- (4) Classifying public lands for waterpower potential.
- (5) Mapping the earth's gravity field.
- (6) Definition of temporal change in groundpoint elevation or position:
 - (a) Subsidence in and around producing oil fields, geothermal reservoirs, and heavily pumped areas of continuing water withdrawal.
 - (b) Open-pit and strip-mine mineral extraction and land reclamation.
 - (c) Volcano inflation, faulting, landslides, and beach and slope erosion.

APT System Configuration

The airborne-instrument package (Figure 1) consists of a three-gimbaled inertial platform to define the position of the aircraft in three coordinates. A two-axis laser tracker is mounted on the same base as the inertial platform in order to update the long-term drift of the inertial platform. Three or more surveyed retroreflectors interspersed with several unlocated retroreflectors provide ground truth. The inertial platform and laser tracker provide the high-accuracy position datum. A laser profiler, to provide line scans of the terrain, is provided for those applications requiring terrain profiling information. However, the three-coordinate reference system may be used with other systems such as scanning lasers or radars, side-looking radar, aerial cameras, and radiometers. The laser altimeter or profiler is just one of a number of equipments that may be used in conjunction with the position and attitude measurement system. An airborne digital computer accepts data from the three sensors and performs the necessary computations and data processing for alignment of the IMU, and position or velocity updating calculations from range and angles. In addition, the computer outputs data to the magnetic-tape recorder and display unit.

The initial flight test configuration will differ somewhat from Figure 1. The purpose of the initial flights is to basically prove the concept, i.e., locate the position of unsurveyed retroreflectors with respect to three surveyed retroreflectors. The basic differences in this initial flight configuration compared to the configuration depicted in Figure 1 include the fact that the profiler will be hard-mounted (the angular errors from the profiler laser beam will be computationally corrected). Interfaces for leveling the profiler platform and reading its gimbal angles are provided, however, so that a stabilized profiler platform may be added in the future. Another difference in the initial flight configuration is that the autopilot/guidance function indicated in Figure 1 will not be implemented. Finally, the indicated Kalman filter update, combining tracker and IMU data, will not be performed in real time. Tracker and IMU data will

Proc. of the 9th GEOP Conference, An International Symposium on the Applications of Geodesy to Geodynamics, October 2-5, 1978, Dept. of Geodetic Science Rept. No. 280, The Ohio State Univ., Columbus, Ohio 43210.

* Under contract 14-08-0001-14578

be recorded in flight, and filtering of the data will be performed post-flight. A simple reset of position and velocity will be performed in real time, however, so that the acquisition time of a new retroreflector is minimized.

A mechanical schematic (Figure 2) of the system shows the geometric relationship and functions of the gimballed subassemblies. The IMU and tracker are mounted in a common housing. The profiler-vertical camera assembly is hard mounted to the aircraft, but referenced to the IMU pitch and roll isolation axes to account for motion of the aircraft.

The IMU consists of a stable member which houses three high-performance gyros and three accelerometers along with their associated electronics. Outside the stable member are three servo-driven isolation gimbals (azimuth, elevation, and roll, in that order) isolating the instruments from aircraft rotation. The support structure surrounding the isolation gimbals is designed so that the tracker assembly mounts directly to its base, thereby providing a physical tie between the structure of the inertial reference system and the tracker pointing axes.

The IMU has a unique thermal-control system which isolates the inertial instruments from the aircraft environment. The gyro mounting surfaces are held at approximately $46.1 \pm 0.05^\circ\text{C}$ and the accelerometer mounting surfaces are held at approximately $43.3 \pm 0.05^\circ\text{C}$. This is accomplished by mounting the inertial instruments directly to the stable member air-cooled heat exchanger and employing thermal shims and individual controllers where necessary.

An X, Y, Z coordinate frame fixed to the inner, or stable, member of the IMU provides the attitude datum. This frame is called the indicated frame, platform frame, or "p" frame. It is initially established during a ground-alignment process, consisting of leveling and gyrocompassing. During leveling, the $X_p - Y_p$ plane is established normal to the local gravity vector. During gyrocompassing, the Y_p axis is established normal to the earth's rotation vector. The process of calibration and alignment of an inertial navigation system is a complex subject in its own right. A preliminary exposition of this process for the APT system is given in Reference 1.

In the IMU, the sensitive axes of the accelerometers are fixed in a known orientation with respect to the three coordinate axes of the "p" frame. The outputs of the accelerometers are integrated twice in the computer to obtain position data for navigation, and converted to latitude and longitude. The "p" frame is maintained when in flight by torquing signals proportional to the computed change in geodetic latitude and longitude. Thus, the platform is driven to maintain its attitude (except for errors) with respect to the normal gravity field of the earth and not the actual gravity field of the earth. It is this property of an IMU which allows the measuring of changes in the deflection of the vertical, a point discussed in detail in Reference 2. In an error-free IMU, one would have a completely self-contained instrument capable of giving position, velocity, and direction of the normal gravity vector in real time.

The inertial system is a low-noise datum at high frequencies, capable of providing base-motion isolation from maneuvers or wind gusts. The inertial

sensors (gyros and accelerometers) suffer from long-term drift, however, and cause errors in the low-frequency portion of the spectrum. To minimize these long-term drifts, the inertial components selected are high-performance instruments developed for an Air Force missile application.

Even with the most accurate inertial systems, it is necessary to obtain updating from ground truth in order to reach the specified precision. To provide high-accuracy position updates, a laser tracker is employed. The tracker makes a vector measurement to a surveyed retroreflector; range and two angles are measured. A minimum of three retroreflectors, not in a straight line, are required in a 3- by 30-km area. The high-frequency information from the inertial system is optimally combined with the low-frequency information from the tracker to obtain an estimate much better than either. The statistical techniques employed for the optimum filtering of the data are given in the following section. It can be shown that the important system errors, including position errors and platform misalignments, are independently observable.

The laser tracker and laser profiler employ pulsed-laser ranging techniques. Distance is determined by measuring the round-trip time of a transmitted laser pulse. Pulsed gallium arsenide lasers are used as the transmitters for both devices. Constant fraction techniques are employed in the receiver threshold detectors to minimize timing errors due to received pulse-amplitude variations. In the profiler, pulse-selection techniques are employed to maximize the number of valid returns from terrain. The tracker contains a beam-splitter to separate the ranging and tracking functions. A four-quadrant detector is used to provide the error signals to the gimbal servos of the tracker. A precision time-interval counter is multiplexed between the profiler and tracker to provide the range measurements.

A control and display unit enables the operator to sequence the system through its various operating modes and to monitor and observe the status of the system. The system may also be sequenced automatically by the computer. Various system characteristics, including temperatures of inertial and other key components, critical voltages, and operational modes are observed through the use of the control panel, as well as by computer monitoring. Steering information for the pilot to fly the desired courses for obtaining the required data is provided.

Several military and commercial-type computers were investigated. For the APT system, the selected computer is the NORDEN PDP-11/70M, which has the speed, memory size, input/output capability, instruction repertoire, architecture, and software support necessary for the mission.

Equations for Navigation and Topographic Profiling

The first implementation of APT will be to prove the concept by performing only one mission, topographic profiling, from the list given in the Introduction. The same APT hardware, in the same aircraft, with the same on-board real-time software can perform the rest of the tasks by using different ground-based post-processing algorithms and

possibly different operational procedures. In this section the algorithms needed for the solution of the primary APT functions, navigation and profiling, are presented.

When the aircraft reaches the survey area, two passes are made over three previously surveyed retroreflectors, deliberately chosen or placed not in a straight line. Range and angle data are obtained by the laser tracker in these passes by sightings on each retroreflector in sequence. These data are used to update and calibrate the position and orientation of the inertial system in preparation for the profiling part of the mission. The positions of any unsurveyed retroreflectors previously placed to satisfy any recognized need for added ground-truth references are determined relative to the surveyed retroreflectors during the initial flight passes. Thereafter, each retroreflector serves as a known reference point and may be tracked to obtain updating data as needed during the profiling phase of the mission.

Figure 3 shows the flow of information through the onboard digital computer of the APT system. The input quantities shown are the profiler range; the three accelerometer velocity readouts and three gimbal angles from the IMU subsystem; and the two tracker gimbal angles and range to the retroreflector from the tracker subsystem. The rates at which each of these quantities is sampled are indicated.

The profiler subsystem data are sampled, time-tagged, and subjected to reasonableness checks to eliminate signal dropouts and returns from the tops of foliage. The slope and intercept of the best-fit straight line are computed from 40 ms of those data which pass the reasonableness checks. The effect of the curve fit is to act as a low-pass filter of the profiler data.

The IMU navigation subsystem samples accelerometers for 80 ms (16 vector samples). The vectors are averaged and time-tagged at the mid-point of the data-acquisition interval. The effect of the averaging is to provide a simple low-pass filter on the input signals, in order to suppress further any aircraft vibration not taken out by the shock-mounting of the IMU assembly. Next, the acceleration vector is rotated by a fixed matrix to compute the north, east, and down components of acceleration, \vec{A} , since the three orthogonally disposed accelerometers are mounted on the stable platform so as to receive equal components of gravity, \vec{g} , as indicated in Figure 2.

Equation (1) is the IMU navigation algorithm.

$$\ddot{\vec{R}}_{IMU} = \vec{A} + \vec{g} - 2\vec{\omega} \times \dot{\vec{R}}_{IMU} - \dot{\vec{\omega}} \times \vec{R}_{IMU} \quad (1)$$

where \vec{R}_{IMU} is the position of the aircraft. This equation is solved, in the "p" frame above for $\dot{\vec{R}}_{IMU}$ and \vec{R}_{IMU} , by using trapezoidal rule integration with a time step of 80 ms. The $\vec{\omega}$ vector is the angular velocity of the stable platform with respect to inertial space, given by Eq. (2)

$$\vec{\omega} = \begin{bmatrix} (\Omega + \dot{\lambda}) \cos \lambda \\ \dot{\phi} \\ -(\Omega + \dot{\lambda}) \sin \lambda \end{bmatrix} \quad (2)$$

where Ω = sidereal earth rate.

$\dot{\lambda}$ = the longitude rate.

$\phi, \dot{\phi}$ = the latitude and latitude rate.

The \vec{g} vector in Eq. (1) is a function of position $\vec{g} = \vec{g}(\vec{R}_{IMU})$ and is given by the output of a gravity model; for example, the WGS72 ellipsoid. An error in position thus generates an error in \vec{g} which, through integration of Eq. (1), generates more error in position. This feedback causes the characteristic 84-minute oscillations of error in the horizontal channels, and the characteristic doubling of the error in the vertical channel every 395 seconds. It is important to note, in this context, that one must use a gravity model to separate the earth's gravitational field from aircraft accelerations. The inertial instruments obey Einstein's fundamental principle of the equivalence of gravity and acceleration in a reference coordinate system; they sense only the linear combination of the two. In what follows, we shall see that the laser tracker measurements, being referenced to the outside world, provide the mechanism for separating gravitational acceleration from nongravitational acceleration.

The data from the tracker subsystem are sampled at high rates, low-pass filtered, and the tracker navigation equation, Eq. (3) is solved for \vec{R}_{lt}^p .

$$\vec{R}_{lt}^b = C_s^b \cdot C_x(\theta) \cdot C_y(\rho) \cdot \begin{bmatrix} 0 \\ 0 \\ -r \end{bmatrix} + \vec{d}^b$$

$$\vec{R}_{lt}^p = C_z(-\alpha) \cdot C_y(-\beta) \cdot C_x(-\gamma) \cdot \vec{R}_{lt}^b \quad (3)$$

In Eq. (3) the tracker range r is rotated about the y -axis for the inner tracker gimbal angle ρ ; then rotated about the x -axis for the outer tracker gimbal angle θ ; then rotated by a fixed orthogonal matrix C_s^b for the alignment of the tracker assembly respect to the aircraft; then translated for the fixed distance, \vec{d}^b , from tracker assembly to IMU; and then rotated about the x , y , and z axes for the outer, middle and inner IMU gimbal angles, respectively. The result \vec{R}_{lt}^p is the distance from the retroreflector to the aircraft in platform (or "p" frame) coordinates.

The IMU provides a slowly drifting (but smooth) navigation estimate at all times. The tracker provides a noisy but nondrifting navigation estimate for short intervals of time (30 to 60 seconds) during which a retroreflector is within a 60° cone of visibility determined by the tracker viewing hole in the floor of the aircraft. As mentioned previously, the data from each of the navigators will be recorded for post-processing on the first flight trials. The algorithms in this section

which are used to process these data, however, are the same whether done in real time or after the fact. The rest of this paper proceeds with the description of the real-time implementation of data processing.

The next step is to mix the data from the two subsystems.

$$\vec{D} = (\vec{R}_{IMU} - \vec{R}_{rr})^1 - \vec{R}_{lt}^p \quad (4)$$

By taking the difference between the positions indicated by the two navigators, as given by Eq. (4), the aircraft motion is subtracted out and there remains only a vector which contains a linear combination of the errors in the two subsystems. The vectors \vec{D} are then accumulated over a 2-second interval (25 vectors), and low-pass filtered again. The 2-second sample then represents input to a Kalman filter, or optimal estimation algorithm as described in Reference 3, Chapters 3 and 4.

A Kalman filter is specified very briefly by listing the elements of the state vector \vec{x} , giving the system dynamics matrix F, the system measurement matrix H, and the measurement covariance matrix R, and the spectral density matrix Q.

The state vector \vec{x} consists of 20 elements.

These are:

- \vec{e} = a linear combination of IMU position error and retroreflector survey error (3 elements)
- $\dot{\vec{e}}$ = IMU velocity error (3 elements)
- $\vec{\psi}$ = vector of stable-platform misalignment angles (3 elements)
- \vec{B}_a = a linear combination of accelerometer bias, vertical accelerometer scale-factor error, and gravity model bias error (3 elements)
- \vec{c} = a linear combination of the constant component of gyro drift and the along-track gravity gradient errors (3 elements)
- $\vec{\eta}$ = a linear combination of various body-axis-fixed constant angle errors (3 elements)
- η_4 = the bias error in the inner tracker gimbal (1 element)
- δr = the bias error in the tracker range measurement (1 element)

Other elements which may be added to the state vector include:

- (1) The position coordinates of unsurveyed retroreflectors.
- (2) Unknown values of gravity disturbance vectors and gradients at a point where a retroreflector is located.
- (3) The gravity gradients and even rate of change of gradients averaged over the flight trajectory.

The present state of development of the software includes the above 20 elements, which suffice to account for all the APT instrumentation errors.

This state vector \vec{x} satisfies a linear differential equation $\dot{\vec{x}} = F\vec{x} + \vec{v}$, where the system dynamics matrix F is a 20 x 20 matrix which is partitioned as follows:

$$F = \begin{bmatrix} F_1 & F_2 \\ 0 & 0 \end{bmatrix} \begin{matrix} 9 \text{ rows} \\ 11 \text{ rows} \\ 9 \text{ cols} \quad 11 \text{ cols} \end{matrix}$$

where . . .

$$F_1 = \begin{bmatrix} 0 & I & 0 \\ S_d - \dot{W} - W^2 & -2W & \ddot{R} - g \\ 0 & 0 & -W \end{bmatrix} \begin{matrix} 3 \text{ rows} \\ 3 \text{ rows} \\ 3 \text{ rows} \\ 3 \text{ cols} \quad 3 \text{ cols} \quad 3 \text{ cols} \end{matrix}$$

$$F_2 = \begin{bmatrix} 0 & 0 & 0 \\ I_3 & 0 & 0 \\ 0 & I_3 & 0 \end{bmatrix} \begin{matrix} 3 \text{ rows} \\ 3 \text{ rows} \\ 3 \text{ rows} \\ 3 \text{ cols} \quad 3 \text{ cols} \quad 5 \text{ cols} \end{matrix}$$

In order to build this F matrix, take \vec{W} and \ddot{R} from Eq. (2) and \vec{R} from the accelerometers. The notation used is that an underscore denotes the 3 x 3 anti-symmetric matrix associated with a given vector, and

$$S_d = \frac{g}{R_e} \begin{bmatrix} -1 & 0 & 0 \\ 0 & -1 & 0 \\ 0 & 0 & +2 \end{bmatrix}$$

where R_e = radius of the earth

g = nominal magnitude of gravity

In the differential equation $\dot{\vec{x}} = F\vec{x} + \vec{v}$, the (20 element) vector \vec{v} is called the plant noise. Spectral-density plots of laboratory measurements taken from actual APTS instruments revealed that a suitable model of the statistics of \vec{v} is zero mean, Gaussian noise with a covariance matrix, called the Spectral Density Matrix, Q.

$$\xi(vv^T) = Q = \begin{bmatrix} \sigma_p^2 & 0 & 0 & 0 \\ 0 & \sigma_v^2 & 0 & 0 \\ 0 & 0 & \sigma_a^2 & 0 \\ 0 & 0 & 0 & 0 \end{bmatrix} \begin{matrix} 3 \text{ rows} \\ 3 \text{ rows} \\ 3 \text{ rows} \\ 11 \text{ rows} \\ 3 \quad 3 \quad 3 \quad 11 \\ \text{cols} \quad \text{cols} \quad \text{cols} \quad \text{cols} \end{matrix}$$

It is possible to show (see Reference 4 page 64) that the vector \vec{D} in Eq. (4) is, to first order, linear in the elements of the state:

$$\vec{D} = \vec{e}$$

$$\begin{aligned} & - R_{1t}^P \vec{\psi} \\ & + R_{1t}^P \left[C_z(-\alpha) \cdot C_y(-\beta) \cdot C_x(-\gamma) \right] (\eta_1, \eta_2, \eta_3)^t \\ & + R_{1t}^P \left[C_z(-\alpha) \cdot C_y(-\beta) \cdot C_x(-\gamma) \right] \left[C_s^b \cdot C_x(\theta) \cdot \vec{j} \right] \eta_4 \\ & - \text{unit}(\vec{R}_{1t}^P) \delta r \\ & + \vec{n}_{1t} \end{aligned}$$

$$\text{i.e., } \vec{D} = \vec{Hx} + \vec{n}_{1t}$$

. . . where the time-varying \vec{H} matrix has 3 rows and 20 columns. The vector \vec{n}_{1t} is the measurement noise in the laser tracker. Since five gimbal angle measurements and one range measurement are used to compute the tracker position (see Eq. (3)); since an angle error affects the tracker position perpendicular to the line from aircraft to retro; since a range error is along that line; and under the assumption that the angle errors are uniformly distributed; then, it is concluded that

$$R \equiv \xi(\vec{n}_{1t} \cdot \vec{n}_{1t}) = \sigma_{\text{range}}^2 (\vec{uu}^t) + \frac{5}{2} r^2 \sigma_{\text{angle}}^2 (I - \vec{uu}^t)$$

where σ_{range}^2 = the variance in range measurements.

σ_{angle}^2 = the variance in angle measurements.

$$\vec{u} = \text{unit}(\vec{R}_{1t})$$

$$r = |\vec{R}_{1t}|$$

This completes the brief description of the Kalman filter.

Referring again to Figure 3, the Kalman filter provides estimates \vec{x} of the state and estimates P of the state covariance every 2 seconds. These estimates may be combined with the IMU data to produce a best estimate $\vec{R}_{a/c}$ of aircraft position.

If the aircraft has acquired data from at least three retroreflectors not in a straight line, and

the quantities \vec{e} , $\hat{\vec{e}}$, $\hat{\vec{\psi}}$ (the first nine elements of the state) are significantly different from zero (using a 3σ test based on the square root of the diagonal of the covariance matrix), then Eq. (5), is used; otherwise, the best estimate is considered to be the uncorrected IMU data.

$$\begin{aligned} \vec{R}_{a/c} &= \vec{R}_{\text{IMU}} - \vec{e} - \hat{\vec{e}}(t - t_0) - \hat{\vec{e}}(t - t_0)^2/2 \\ \vec{V}_{a/c} &= \vec{V}_{\text{IMU}} - \hat{\vec{e}} - \hat{\vec{e}}(t - t_0) \\ \vec{A}_{a/c} &= \vec{A}_{\text{IMU}} - \hat{\vec{e}} \end{aligned} \quad (5)$$

where $\hat{\vec{e}}$ and $\hat{\vec{\psi}}$ = state elements
 $\hat{\vec{e}}$ = obtained from $\hat{\vec{x}} = \vec{F}\vec{x}$

t_0 = the time of the most recent Kalman filter update, so that $(t - t_0) < 2$ seconds

The corrected aircraft navigation data from Eq. (5) are used to build the state dynamics matrix F in the the Kalman filter, and \vec{W} and \vec{W} or Eq. (2). \vec{W} is the gyro torque rates used to locally level the stable platform.

Finally, the position of the aircraft $\vec{R}_{a/c}$ from Eq. (5) can be combined with the profiler data to obtain elevation and position at the nadir. Since the profiler will be located several feet from the IMU, it will be measuring the elevation of a point which is displaced horizontally from $\vec{R}_{a/c}$ and which (in general) will thus have an elevation different from the IMU, depending upon aircraft pitch and roll angles. The geometry of the aircraft gives (in locally level coordinates)

$$\vec{R}_{\text{alt}} = \vec{R}_{a/c} - (I - \vec{\psi}) \cdot C_z(-\alpha) \cdot C_y(-\beta) \cdot C_x(-\gamma) \cdot \vec{p}^b$$

where \vec{R}_{alt} = position of the profiler.

$\vec{R}_{a/c}$ = position of the IMU.

$C_z(-\alpha), C_y(-\beta), C_x(-\gamma)$ are the same rotation matrices, dependent on IMU gimbal angles α, β and γ that are defined in Eq. (3).

\vec{p}^b = the distance of the profiler from the IMU in aircraft body-axis coordinates.

This leads to the actual survey datum:

$$(x_{\text{alt}}, y_{\text{alt}}, z_{\text{alt}} + \hat{h})^t = \vec{R}_{\text{gr}} \quad (6)$$

where $x_{\text{alt}}, y_{\text{alt}}, z_{\text{alt}}$ are the north, east, and down components of \vec{R}_{alt} .

Computer Simulations

In order to verify the APT system concepts, there is an on-going effort to exhaustively model all the dynamics and statistics of a typical APT mission on a digital computer. The strategy is: (1) to write an off-line non-real-time version of the navigation and profiling estimation equations given in the previous section, called an estimation model; (2) to write a more exhaustive, second-order simulation of the APT system error dynamics, called a truth model; and (3) to compare the outputs of the estimation model (estimates of the state \vec{x}) with the inputs \vec{x} to the truth model, the residuals giving a realistic estimate of the eventual APT performance. Figures 4 and 5 illustrate the use of the APT truth model and estimation model. At their current stage of development, both computer programs can give a realistic estimate of the amount of error contri-

buted by the APT instruments themselves. The programming for component of error contributed by residual gravity model errors is not yet complete, however, and so will be accounted for later in this section by another technique.

In a typical computer run, we simulated a 20-minute section of a nominal APT mission with the truth model. The simulation flew the aircraft over the trajectory indicated in Figure 6, wherein the three circles represent the region of visibility around three perfectly surveyed retroreflectors. The retros are about 10 km apart, the aircraft has a mean speed of 53 1/3 m/s, a mean altitude of 0.91 km, and the viewing hole for the tracker defines a 60° cone of visibility. In this simulation the laser accuracy, after low-pass filtering for 1 second, was 3 cm in range, 22 μ sec (about 0.107 mrad) in pointing. The IMU performance was based on parameters and spectral models derived from classified military data taken on instruments identical to the APT accelerometers and gyros. The truth model program simulated the aircraft dynamics, IMU error drift, laser measurement errors, and retroreflector geometry, but not the laser profiler or the gravity disturbance vector.

The 20-state Kalman filter described previously was used as an estimation model on the data generated by the truth model. For each state the residual error was computed as a function of time, and plotted. The Kalman filter fluctuates wildly for the first part of the flight, until data from three different retroreflectors (not in a straight line) have been processed, and the filter achieves geometric sufficiency. Accordingly, Figures 7 and 8 corresponding to the vertical position and acceleration error, respectively are plotted only for the last 700 seconds of the 20-minute flight. On each graph, three curves are plotted. A middle curve representing the state-element residual estimation error is enclosed by an envelope corresponding to $\pm 1.6 \sigma$ (90% confidence), where σ is computed by the Kalman filter as the square root of the appropriate diagonal element of the estimated covariance matrix P.

In Figure 7, we plot the vertical position error in cm. Since the error curve fills, but remains inside, its 90% envelope most of the time, we may say that the Kalman filter is a self-consistent model when driven by this truth model data. Qualitatively, the curve and envelope show characteristic periods of compression and expansion corresponding to the aircraft being inside or outside a retroreflector cone of visibility. When outside a cone of visibility, the envelope expands as time to the 3/2 power. 90% of the errors are less than 8 cm. This figure represents the fundamental surveying error from the APT instruments; however, if surveyed retroreflectors were placed closer together, then we might expect even better performance.

In Figure 8, the vertical acceleration error is plotted in mgals. It can be seen that the filter is still converging at the end of 20 minutes, however, 90% of the data are already within a 0.1-mgal band. What we have shown here is the ability to determine the mean gravity anomaly over the region (actually averaged over the trajectory of the aircraft) to within 0.1 mgal absolute accuracy. More sophisticated modelling will allow determination of mean gravity gradients over the region, or mean

gravity gradients between any pair of retroreflectors or values of gravity disturbance vectors above each retro at the height of the aircraft, all to within an absolute accuracy of 0.1 mgal. Placing more retroreflectors will extend the region of the gravity survey beyond the simulated 30 km; placing them closer together will increase the resolution of a gravity survey better than the simulated 1 point in 30 km.

The other 18 state elements were plotted in a similar format, yielding information on navigation, horizontal retroreflector survey error, deflection of the vertical, gyro drift, APT system mechanical misalignments, IMU platform attitude error, and laser tracker errors. These results will be published in January 1979.

So far only the APT instrumentation errors have been simulated. A back-of-the-envelope computation was carried out using gravity anomaly data from the Denver area supplied by the Department of the Interior, Geological Survey, to demonstrate the feasibility of correcting for the effects of gravity anomalies. The study consisted of calculating position errors attributable to residual gravity errors along a 30-km flight path by integrating twice. It was assumed that the aircraft would fly along the path at a constant velocity of 53.3 m/s, resulting in a 600-second flight. The initial position and velocity errors were assumed to be zero and these errors were again set to zero each time it was necessary to simulate the effect of three laser tracker updates. In addition, it was assumed that measurements of gravity anomalies were known a priori, or could be estimated, at three retroreflectors located along the flight path at 13-km intervals. Based on these three measurements, a quadratic model for the gravity data was chosen and the coefficients of the model were computed. The difference between the known gravity anomalies and the gravity values obtained from the quadratic model were considered to be the residual gravity errors and thus the cause of position errors.

The result of this study was that the standard deviation associated with the vertical position errors was 6.1 cm, the maximum error was 21 cm, 90% of the vertical position errors were bounded by 12 cm.

Although this study represents only a first cut at the gravity problem, it suggests that a combination of modeling, estimation, and a priori measurements should be sufficient to account for gravity anomaly errors in the APT system.

Since the vertical error from instrumentation is within a 90% confidence interval of 8 cm, since the unsimulated gravity disturbances will be about 12 cm, and since these are uncorrelated, then

$$\text{RSS error bound} = \sqrt{8^2 + 12^2} < 15 \text{ cm}$$

Crustal Movement Monitoring

In the preceding section, the capability of the APT system to perform real-time navigation and topographic profiling to an accuracy of 15 cm in the vertical, relative to three control points, was demonstrated in a survey area about 30 x 3 km. For those applications where the survey region has been chosen to straddle a fault line and where one plate

has moved relative to another by more than 15 cm, the APT system could be used, unmodified, by the simple expedient of placing all three control points on the same plate; differencing the profiler elevations taken on an APT survey at time t_0 from an APT survey taken at time t_1 ; and averaging the differences on each plate separately to remove bias errors and the effect of not repeating the aircraft path exactly. If $\bar{Z}_J(t_k) - \bar{Z}_J(t_0)$ is the average of APT vertical displacement measurements of plate J at time t_k , then the vertical movement of plate 1 with respect to plate 0 during the time from t_0 to t_1 is:

$$\overline{[Z_1(t_1) - Z_1(t_0)]} - \overline{[Z_0(t_1) - Z_0(t_0)]}$$

There are some problems with this method: resolution, extent of survey area, and accuracy. By modifying the APT system slightly we can solve these problems.

First of all, the resolution problems can be solved by eliminating the profiler. Profiling data is taken every 40 ms (i.e., 3 meters) then has to be averaged over the aircraft trajectory to give a resolution meaningful for crustal plate dimensions. Also, profiling data will not be exactly the same in successive surveys, since the aircraft can not repeat its flight path exactly; hence, the survey area has to be profiled densely so that the averages $\bar{Z}_J(t_k)$ are representative of the area. Lastly, the laser tracker can be used as a more effective surveying device than the profiler. This can be accomplished by inverting Eq. (3) and (4) and solving for \vec{R}_{rr} . Instead of using measured tracker range and pointing angles with a known retroreflector position to compute the aircraft position, the aircraft position is assumed known and the rotation and translations performed to compute the location of the retroreflector. The accuracy will be as good as the IMU subsystem navigation accuracy. The aircraft needs to repeat its trajectory from survey to survey only well enough to enter the cone of visibility of the retroreflectors. Retroreflectors can be placed atop fixed monuments in a grid at whatever spacing corresponds to meaningful resolution of crustal movement measurements. If $\vec{R}_J(t_k)$ is the APT surveyed position of retroreflector J at time t_k , then the movement of retro J with respect to retro I from time t_0 to time t_1 is

$$[\hat{\vec{R}}_J(t_1) - \hat{\vec{R}}_I(t_1)] - [\hat{\vec{R}}_J(t_0) - \hat{\vec{R}}_I(t_0)] \quad (7)$$

Notice that we compute vector displacement, not just the vertical component.

The problem of survey extent was related to survey accuracy. As mentioned in the previous section in reference to Figure 7, position errors in the IMU grow as time to the 3/2 power when there are no tracker measurements. One way to increase the size of the survey area is to fly faster so that more distance can be covered for a given error bound. In a jet aircraft, speeds of 266.7 m/s, or five times the speed assumed in the previous section, may be assumed. Such speeds imply a higher safe operating altitude, say 4.5 km.

The problem of accuracy was addressed by a computer simulation of the APT system in which an air-

craft was flown at a height of 4.5 km, at a speed of 266.7 m/s, repeatedly around a closed, oval traverse about 120 km long and 30 km across. At each end of the oval was a cluster of three surveyed retroreflectors about 20 km apart in a right triangle configuration. The clusters were about 100 km apart, and the complete traverse could be flown in 20 minutes. The parameters for the laser tracker were the same as for the profiling mission. If the navigation error from this simulation is observed, we get a measure of the ability of APTS to survey in retroreflectors. In this simulation we did not include the effects of unmodelled gravity errors on the system, because these may be reduced to residuals by availability of a priori gravity surveys, reduced further by the ability of APTS to estimate the gravity field, and removed through the following survey operation. If we fly the same (± 500 m) trajectory at the same speed, then the gravity-induced IMU errors will be the same from survey to survey and subtract out in Eq. (7). Of course, the local gravity field may undergo temporal change also; however, the effect, which is 3.3 microgals per cm of vertical displacement is distinctly second order.

The result of the simulation was that 90% of the errors were less than 18 cm. Such a result shows that the APT could be used for measuring only very large vertical crustal displacements unless further modifications are made. One improvement would be in more sophisticated modelling to use all of the information available. There is a post-processing technique, called back smoothing, (see Reference 3), which is a refinement to the Kalman filter algorithm offering the potential of significant improvement. A forward Kalman filter forms the best estimate of the state vector given initial conditions, the models, and all the measurements up to the time of the estimate. A backward Kalman filter forms the best estimate of the state given final conditions, the models, and all the measurements which occurred after the time of the estimate. An optimally weighted average of the forward and backward filter outputs then forms the optimally smoothed estimate of the state. Under the assumption of $t^{3/2}$ error growth, it is easy to show that the peak error the optimally smoothed estimate is 1/4 the peak error in the Kalman filter estimate. The back smoothing algorithm is very cumbersome, costly of computer and programming time, and yet offers the possibility of measuring crustal movement with the APTS to within about $18 \div 4 = 4.5$ cm.

We shall now discuss modifications to the APT system hardware and improvements to mathematical modelling which would push the APT performance to its ultimate limit. What has been shown, so far, is that the errors derived only from APT instrumentation are about 2.5 times higher for measuring crustal movements (> 18 cm before backsmoothing) than for topographic profiling. This factor occurs because the geometry of the tracker measurements is so much less favorable at the higher altitude and sparser retroreflector spacing used to measure crustal movements. This geometry affects the system through the $t^{3/2}$ error growth between retrosightings and through the degradation in tracker accuracy at higher altitude. The time between tracker position fixes could be shortened only by flying even faster, involving the choice

of a supersonic aircraft; however, it was felt that aircraft maintenance expenses for such a vehicle were not justified by the marginal gain in APT performance.

The degradation in tracker performance with increased altitude occurs for two reasons. First of all, the laser beam must pass through more of the atmosphere, and over a greater range of pressure, temperature, and humidity. Therefore the index of refraction will vary over a greater range along the ray-path, hence (through Snell's Law) there will be more atmospheric ray bending. Because of ray bending both the direction and distance measurements of the tracker are in error. If the APT system were modified so that the tracker were replaced by a two-color laser, then one could correct for the change in arc length due to raybending. The scheme is described in Reference 5. The pointing uncertainties can be reduced to 3 sec by atmospheric modelling of $\delta\theta$ (raybending distortion) versus θ (angle of incidence) as described in Reference 4. The second effect is a purely geometric one. The distance error caused by tracker pointing errors is 1 mm per microradian for each km of altitude. The precision angle readouts, as envisioned for APTS, have $\sigma = 22 \text{ sec}$ effective pointing error. At 0.91 km altitude this corresponds to 10 cm, at 4.5 km to about 0.5 meter. Most of this error is repeatable and could be removed by careful laboratory calibration of a table of $\delta\theta$ versus θ for each precision angle resolver. If this were done the effective pointing error could be reduced by at least a factor of 4 to 5.5 sec .

In the computer simulation which estimated 18-cm accuracy for Eq. (7) (4.5 cm presumed after back smoothing) we assumed all tracker information available for the 100-km flight path (37.5 seconds flying time) between the two clusters of surveyed retros was used for survey and none for navigation. In fact, such navigation information is available, and could be used if more sophisticated modelling were performed; thus, the results of the computer simulation are unduly pessimistic. There are three major sources of navigation data not included in the simulation. First, each retro supplies a velocity measurement with which to update the drifting IMU. The 1600-Hz laser tracker pulse rate gives a complete time history of the aircraft with respect to the retro, and that retro is not moving for the 10^4 seconds of the survey. In fact the measurement equation for a velocity update can be obtained by differentiating Eq. (3) and (4). If one places enough retroreflectors along the survey trajectory, then one simultaneously surveys-in more points for measuring crustal plate movements and supplies almost continuous velocity information to the system. The limit is reached when the retros are so close that the regions of visibility overlap, because it takes 2 or 3 seconds to move the tracker from locking on one retroreflector to the next. The effect of such a near-continuous velocity update on position accuracy should be quite dramatic, since, instead of a characteristic $t^{3/2}$ error growth caused by twice integrating random acceleration errors, one would expect $t^{1/2}$ error growth caused by a single integration of the nondrifting random residual velocity errors. In Reference 4, Chapter 3, Appendix B an estimate of less than 1 cm for $t = 375$ seconds is made assuming a perfect and uninter-

rupted velocity update.

The second major source of navigation information comes from the fact that the crustal motions of closely spaced points will be highly correlated. The correlations, if modelled, would allow the extraction of position information for navigation from redundantly placed retroreflectors.

The third source of information occurs because there is a bandwidth separation of the navigation error and APT survey error which has not been taken advantage of. So far, we have been observing navigation error as though this were the same as survey error. However, the navigation errors are pure functions of time, and the survey displacements which we are attempting to compute are pure functions of latitude and longitude. If one were to repeatedly cross over a retroreflector, then one would expect the IMU error to be statistically independent from crossing to crossing, so that the survey error could be a factor of \sqrt{N} times better than the navigation error, where N is the number of times the retro has been crossed.

Unfortunately, updating the existing APT simulation program with the equations necessary to implement velocity updates and survey computations, does not fit the APT development schedule, priorities, timing, and budget. As mentioned in the previous section, the system will be programmed to perform the tasks of navigation and profiling. What can be done, however, is to use the existing simulation program to infer a best case bound on APT performance. There is already a worst case bound, 4.5 cm with back smoothing, gotten by assuming no tracker information available during an APT survey. The best case bound is gotten by using the existing computer simulation to supply position data from perfectly surveyed retros and observing navigation error. Admittedly the combined effect of velocity updates, survey correlations, bandwidth separation of survey and navigation errors, and back smoothing can not be as good as position updates, but it does set an APT performance limit.

Accordingly, another computer simulation was run, with the IMU model the same as APTS, with the laser tracker pointing accuracy improved to $\sigma = 5.5 \text{ sec}$. Sixteen perfectly surveyed retroreflectors about 16 km apart with a 60° cone of visibility lay along an oval flight trajectory as indicated in Figure 9. The aircraft was flown at 266.7 m/s at an altitude of 4.5 km. The vertical position errors for one traverse of the oval are plotted in Figure 10 in the same format used in Figure 7. In Figure 10, one can see by inspection that most of the errors lie between ± 1.8 cm. This number was confirmed by plotting the points in Figure 10 in an integrated histogram format. In Figure 11, the abscissa is error bound in cm, the ordinate is the % of errors from the simulation less than or equal to the abscissa. From Figure 11 one can read off 1.8 cm as the 90% error bound.

From these computer simulations we have reached the conclusion that the APT system could survey vertical crustal movements much better than 4.5 cm relative to three control points, but cannot survey better than 1.8 cm, in a survey area of diameter 120 km (about $1.5 - 4$ parts in 10^7). The system also has the capacity to measure horizontal displacements to the same order of accuracy.

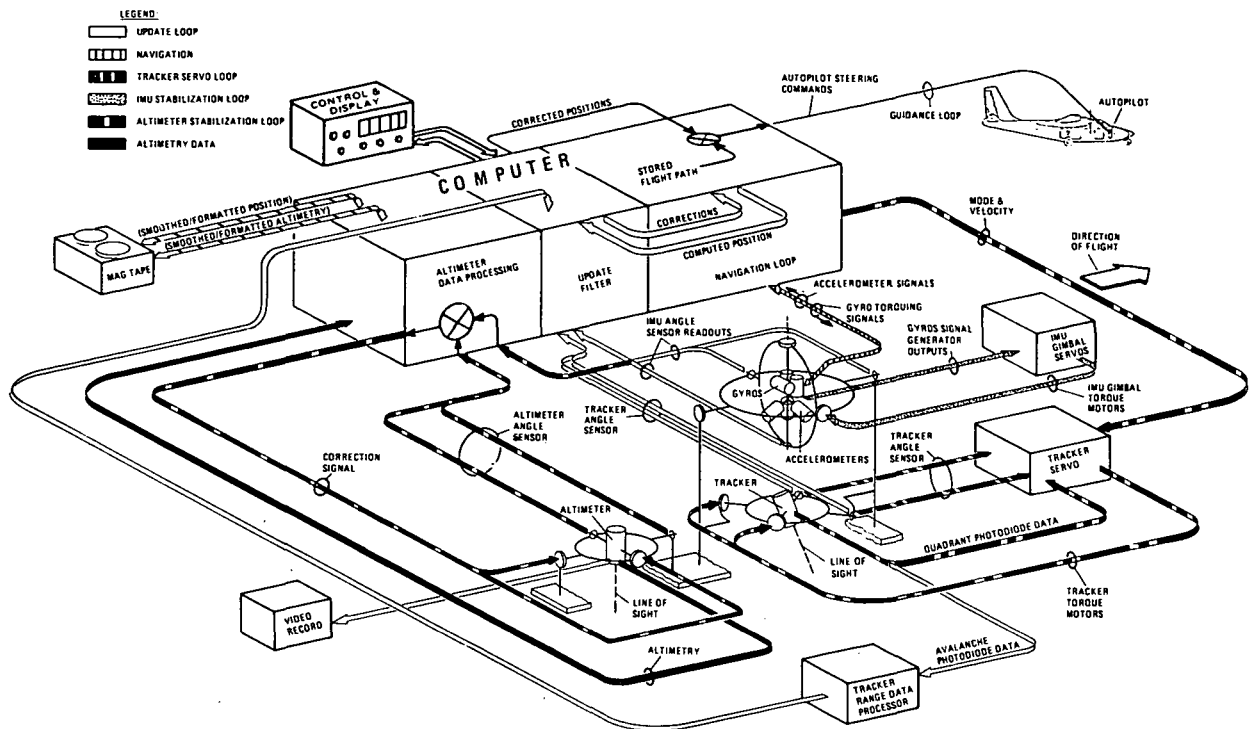


Figure 1. USGS/APTS functional diagram.

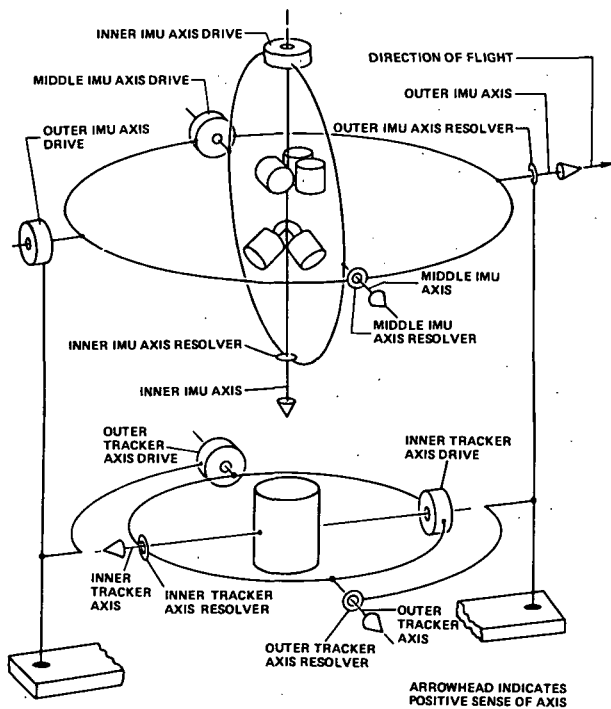


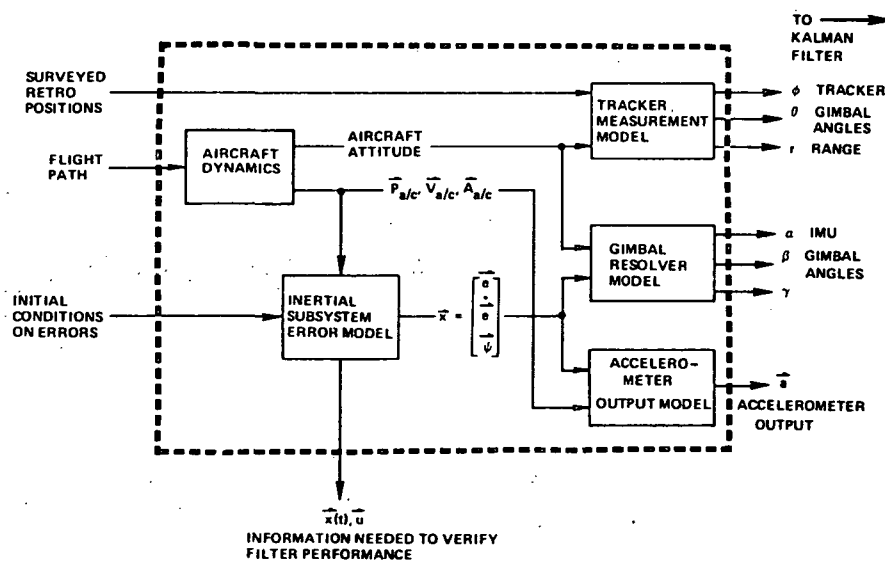
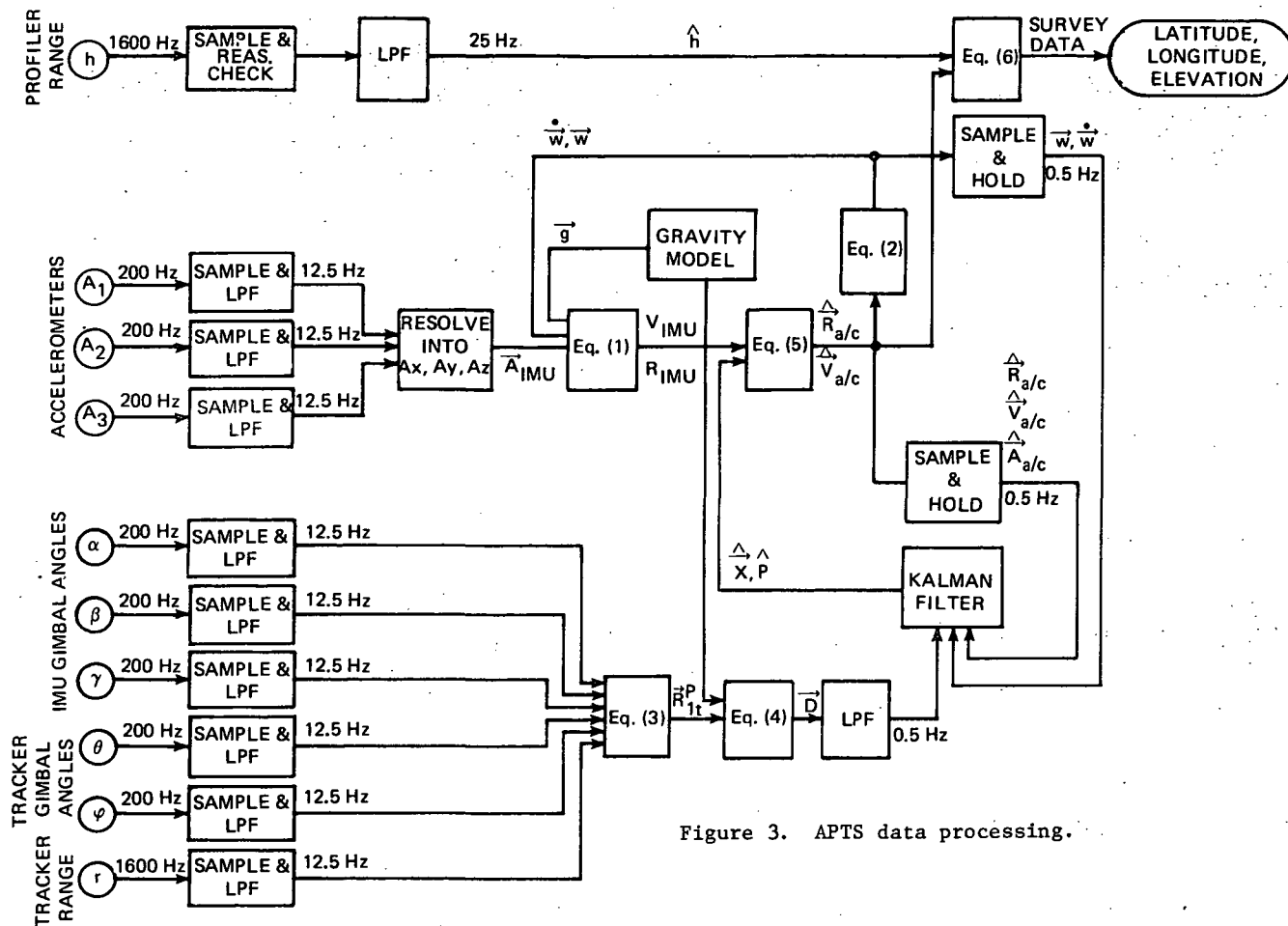
Figure 2. APTS Inertial Measurement Unit (IMU) and laser tracker schematic.

Acknowledgments. This study was made possible through the dedicated work of the CSDL-APTS technical staff. Thanks is especially due to Linda K. Lemos, John H. Barker, Glenn Mamon, and John W. Hursh who are also, to some degree, responsible for the information presented here.

Publication of this paper does not constitute approval by The Charles Stark Draper Laboratory, Inc., of the findings or conclusions contained herein. It is published for the exchange and stimulation of ideas.

References

1. Garofalo, F.J. 1978. APTS-IMU calibration and alignment. Cambridge, MA: The Charles Stark Draper Laboratory, Inc. report R-1193.
2. Schwartz, K.P. 1978. "Accuracy of vertical deflection determination by present-day inertial instrumentation." Presented at Ninth Geodesy/Solid-Earth and Ocean Physics Conference. 2-5 October 1978, at Columbus, OH.
3. Technical Staff, The Analytical Sciences Corp. 1974: Applied optimal estimation. Gelb, A., ed. Cambridge, MA: M.I.T. Press.
4. APTS-CSDL Staff. 1977. Aerial profiling of terrain system design phase, interim report. Cambridge, MA: The Charles Stark Draper Laboratory, Inc., report R-1070.
5. Earnshaw, K.B., and Hernandez, E.N. 1972: "Two-laser optical distance-measuring instrument that corrects for the atmospheric index of refraction." Applied Optics v.11, no.4: 749-54.



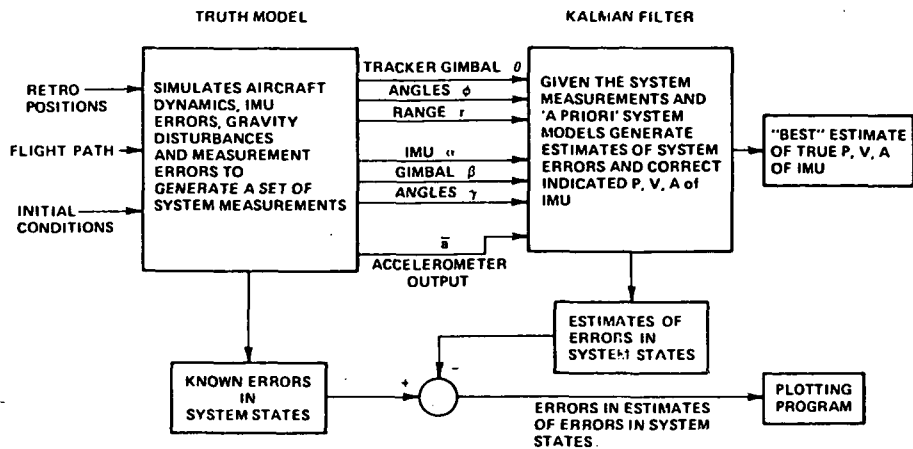


Figure 5. Interaction of truth model and Kalman filter.

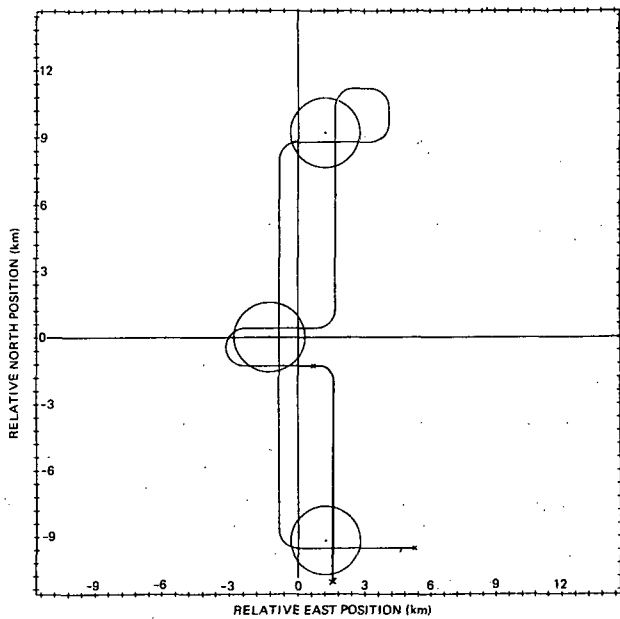


Figure 6. Flight trajectory and retroreflector geometry for computer simulation of APT navigation performance.

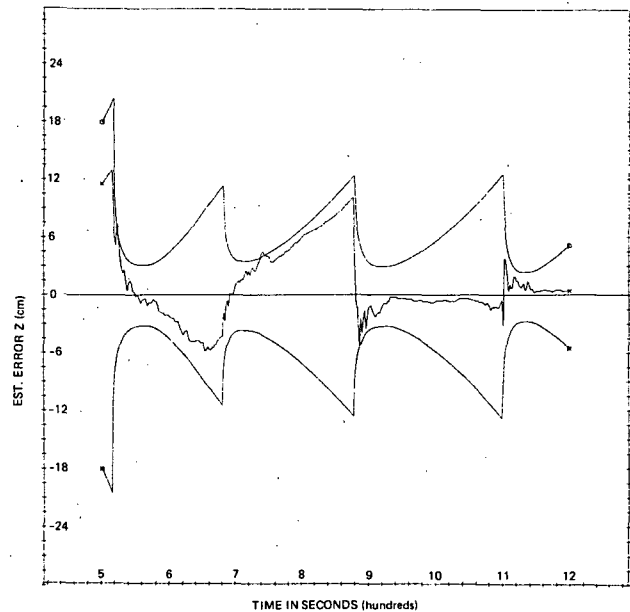


Figure 7. Vertical position error and covariance envelope from navigation simulation.

6. Broxmeyer, C. 1964. Inertial navigation systems. New York: McGraw-Hill.
7. Youmans, D.G. 1977. Flight testing of an airborne laser terrain profiler. Cambridge, MA: The Charles Stark Draper Laboratory, Inc. report R-1106.
8. Carofalo, F.J. and Lemos, L.K. 1978. Aerial profiling of terrain system truth model documentation. Cambridge, MA: The Charles Stark Draper Laboratory, Inc., report R-1182.
9. Soltz, J.A. 1978. APT in-flight navigation equations. Cambridge, MA: The Charles Stark Draper Laboratory, Inc., report R-1192.
10. Hursh, J.W., Mamon, G., and Soltz, J.A. 1977. "Aerial profiling of terrain." In Proceedings: 1st international symposium on inertial technology for surveying & geodesy. pp. 121-30. Ottawa, Canada: International Association of Geodesy, and the Canadian Institute of Surveying.

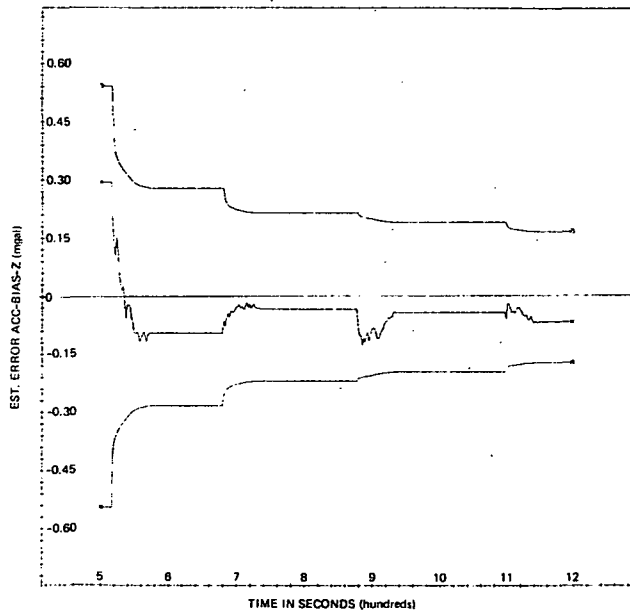


Figure 8. Vertical acceleration error and covariance envelope from navigation simulation.

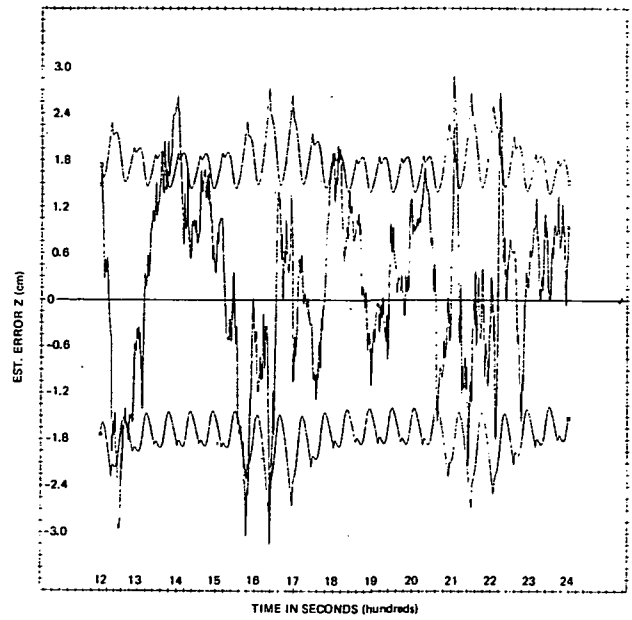


Figure 10. Vertical position error and covariance envelope from crustal-measurement simulation.

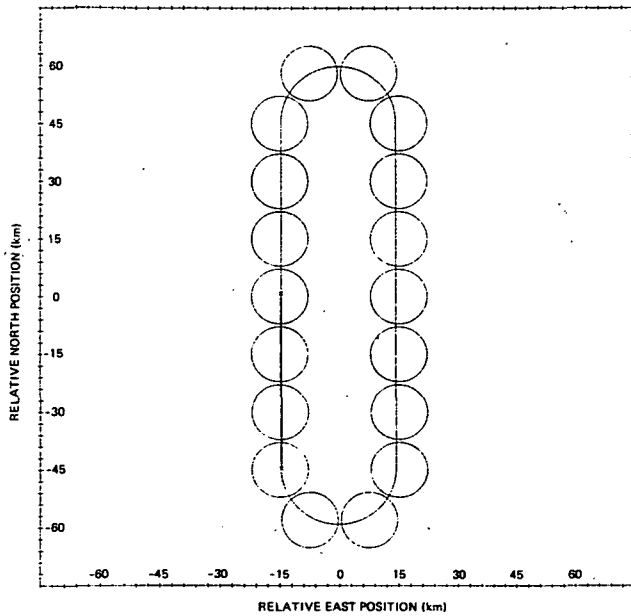


Figure 9. Flight trajectory and retroreflector geometry for simulation of APTS measurement of crustal movements.

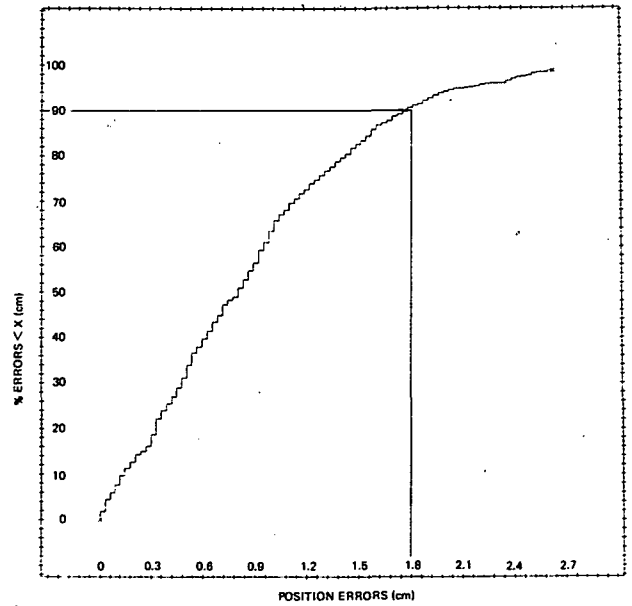


Figure 11. Integrated histogram of vertical position errors from crustal movement simulation.